

# Optical Tweezers

M. Filova<sup>a,\*</sup>, P. Oikonomou<sup>a</sup>

<sup>a</sup>New York University Abu Dhabi

## Abstract

Optical tweezers is an instrument designed to capture small objects with a highly focused laser beam. It is valuable because of its capability to measure displacements at micron scale and piconewton forces. In this experiment we assembled a Modular Optical Tweezers kit from Thorlabs and performed a calibration. Currently, the instrument is not trapping the bead in Z-axis and the focus of the laser does not coincide with the focal point of the objective. Here we report on the displacement sensitivity of the quadrant photodetector which detects the position of a bead in the trap, found at several laser powers for X and Y axis. Then, we report the trap stiffness, found separately for X and Y axis, at several laser powers, by analyzing the time-series of a trapped bead with three methods: power spectrum density, equipartition theorem and potential energy. The trap stiffness was found to be different along X and Y. We also find Boltzmann constant and drag coefficient from the fit parameters to the power spectrum density. The values were not in agreement with literature values indicating possible faults in the PSD analysis or a drag coefficient different than the theoretical one.

## 1. Introduction

Optical tweezers (OT) is an instrument capable of trapping and moving small objects - particles or microspheres (beads) - at all three dimension by applying a single highly focused laser beam. The technique was pioneered in the mid 1980s by Arthur Ashkin, after around 15 years of developing applications of optical forces to small objects. Since then, various technological advances allowed for increased resolution and precision in measurements. Optical tweezers have been of great importance for advancing knowledge in biophysics, especially for the understanding of various biomolecules - the forces they exert, their mechanical properties, the step length of motors. Beyond biophysics, optical traps have applications in other fields too, for example: to trap and characterize gas-filled microbubbles, to assemble and provide power for nanodevices, and to investigate phenomena from statistical physics by trapping biomolecules or nanoparticles [1, 2].

In single molecule biophysics, the importance of OT comes from the ability to make repeated and precise measurements of forces and displacements in active biological systems [3]. The net force applied by the laser is approximately linear near the focus of the laser beam (the center of the trap) and can be modeled as a Hookean spring. Optical tweezers measure the displacement of the trapped particle. A calibration procedure can determine the 'stiffness' of the trap modeled as a spring, which can then be used to convert the measured displacements into forces [4, 5].

In this experiment we have assembled a purchased OT kit, designed for undergraduate lab usage. We report on the specifications of the instrument, the current operation mode and the

performed calibration procedure. The displacement sensitivity of the quadrant photodetector and trap stiffness were found at different laser powers. Additionally, the drag coefficient and Boltzmann's constant were extracted from fit parameters and compared to theoretical values.

## 2. Theoretical Background

In this section we briefly explain the theory behind the working principles of optical trapping. At a high level, it is easy to understand the working principle of optical trapping as the result of conservation of momentum. The refraction of light through the translucent bead, is essentially the bead changing the momentum of the incoming light. Therefore, due to momentum conservation, after the "collision" the bead must impart said momentum change in the opposite direction [6]. As one can imagine, this effect from multiple directions would allow a sufficiently light, bead to be "pushed" towards the center of a laser beam [6]. There is another effect at play here; the effect of radiation pressure. As photons hit the bead, they lose momentum, the lost momentum is picked up by the bead to act as a force towards the direction of light propagation [6]. Hence a balance must be achieved between those two effects in order to trap a body in 3D. The two effects can be seen in Fig. 1

The previous abstract description of the effect, merely serves as a starting point to develop some intuition about the principles of optical trapping. Now let's examine both effects, i.e. (a) Gradient force and (b) Radiation pressure, in a more rigorous manner. The goal of the rest of the section is to obtain the equations of motion of a trapped bead in order to understand the structure of the effective trapping potential.

\*Corresponding author

Email addresses: mf3846@nyu.edu (M. Filova), po524@nyu.edu (P. Oikonomou)

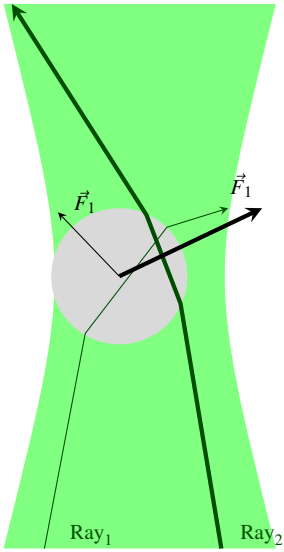


Figure 1: A bead (gray) is off-center from the trap's focal point (light green). The refraction of two arbitrary rays (dark green) is shown, along with the forces each one imparts. The thickness of the ray is proportional to the density of rays passing through a similar path. As is evident, the bead will self correct towards the central position, when all the rays are considered.

### 2.1. Gradient Force

The gradient force, is perhaps the most important of the two forces at play, as it allows to center the bead to the plane perpendicular to the direction of propagation of the laser. In our analysis we will assume that the bead we are trapping is significantly bigger than the wavelength of the laser. We will further assume that the material of the particle can be modelled (at least to first order) as a linear dielectric.

Therefore, when a light ray passes through the bead, it is going to induce a dipole moment  $\mathbf{p} = \alpha \mathbf{E}$  [7]. We will now examine the Lorenz force on this dipole. Specifically, the Lorenz force is given by (1), and we can easily show that applied to a point dipole it transforms to (2) [7].

$$\mathbf{F}_g(\mathbf{r}, t) = q(\mathbf{E}(\mathbf{r}, t) + \mathbf{v}(\mathbf{r}, t) \times \mathbf{B}(\mathbf{r}, t)) \quad (1)$$

$$\mathbf{F}_g(\mathbf{r}, t) = \alpha \left[ (\mathbf{E}(\mathbf{r}, t) \cdot \nabla) \mathbf{E}(\mathbf{r}, t) + \frac{\partial \mathbf{E}}{\partial t} \times \mathbf{B}(\mathbf{r}, t) \right] \quad (2)$$

where  $\mathbf{F}_g$  is the gradient force,  $\mathbf{E}$  and  $\mathbf{B}$  are the electric and magnetic fields of the laser light, and  $\alpha$  is the dielectric polarizability of the bead.

By vector manipulation (2) becomes (3).

$$\mathbf{F}_g(\mathbf{r}, t) = \alpha \left[ \frac{1}{2} \nabla E^2 - \mathbf{E} \times (\nabla \times \mathbf{E}) + \frac{\partial \mathbf{E}}{\partial t} \times \mathbf{B} \right] \quad (3)$$

Assuming that the magnetic field contribution to the motion of the dipole is negligible [8] we obtain (4).

$$\mathbf{F}_g(\mathbf{r}, t) = \frac{\alpha}{2} \nabla E^2(\mathbf{r}, t) \quad (4)$$

Equation (4) is the instantaneous gradient force. We remind ourselves that the electric field has an equation of the form:

$\mathbf{E} = \mathbf{E}_0 \exp(k \cdot \mathbf{r} - \omega t)$ . As a result we need to get the time average of this quantity to obtain the gradient force on the bead. This is done in (5) [8].

$$\mathbf{F}_g(\mathbf{r}) = \langle \mathbf{F}_g(\mathbf{r}, t) \rangle = \frac{\alpha}{4} \nabla I(\mathbf{r}) \quad (5)$$

where  $I(\mathbf{r})$  is the intensity of the light at some point in the medium.

### 2.2. Radiation Pressure

We will now discuss the effect of radiation pressure on the bead. We know that for a perfectly reflective surface the radiation pressure is given by (6) [9].

$$P(\mathbf{r}) = \frac{1}{c} \langle \mathbf{S}(\mathbf{r}, t) \rangle = \frac{I(\mathbf{r})}{c} \quad (6)$$

where  $P$  is the pressure due to radiation,  $\mathbf{S} = \frac{1}{\mu_0} \mathbf{E} \times \mathbf{B}$  is the Poynting vector, and  $I(\mathbf{r})$  is the intensity at some point  $r$  on the beam. However, there is a catch. Our bead is not perfectly reflective, hence we need to correct for the energy that goes through. The correction is referred to as Minkowski's formula and is given by (7)

$$P(\mathbf{r}) = \frac{n}{c} \langle \mathbf{S}(\mathbf{r}, t) \rangle = \frac{n I(\mathbf{r})}{c} \quad (7)$$

where  $n$  is the refractive index of the bead. Hence assuming a cross sectional area  $A_c$  the radiation pressure force can be give by (8).

$$\mathbf{F}_p(\mathbf{r}) = \frac{n A_c}{c} I(\mathbf{r}) \hat{\mathbf{k}} \quad (8)$$

where  $\hat{\mathbf{k}}$  is the direction of propagation of the light.

## 3. Methodology

### 3.1. The instrument

To perform the experiment we first installed an optical tweezers kit - Thorlabs' OTKB(M) Modular Optical Tweezers [10]. In this section we briefly describe the parts and specifications of the instrument. Then we report the problems we faced when assembling the instrument and detail the procedure we used to circumvent the current issues. Finally, we describe the methodology used to perform the instrument calibration.

#### 3.1.1. The setup

*Broad introduction.* An optical trap (OT) is used to measure displacements with  $\mu\text{m}$  precision and measure and apply forces in the  $p\text{N}$  range. To do this, it is necessary to carefully direct the laser light, collect the wanted information and have control over the movement of the sample. The instrument has two light sources: the laser that traps the bead and a white light LED lamp which illuminates the sample to make it visible. As seen on Fig. 2, the instrument is composed of the following parts:

- **stage:** holds the sample and allows to move the sample precisely in all three directions
- **laser diode:** produces the laser beam

- **LED lamp:** produces white light to illuminate the sample
- **beam expander (telescope):** expands the beam coming from the laser diode
- **inverted microscope:** focuses the laser beam on the sample and directs the LED light through the sample
- **quadrant photodiode (QPD):** collects the laser light scattered off the bead and provides a measure of position
- **camera:** collects the LED light and provides an image of the sample
- **data acquisition module:** collects the outputs from the QPD and the strain gauges in the stage, and sends input to the voltage controllers of the piezo actuators in the stage

Therefore, when observing a sample, the following output information is obtained: the location of the sample on the stage read either manually or with the strain gauges, the relative location of the bead in the trap detected with the QPD, and an image of the sample taken with the camera.

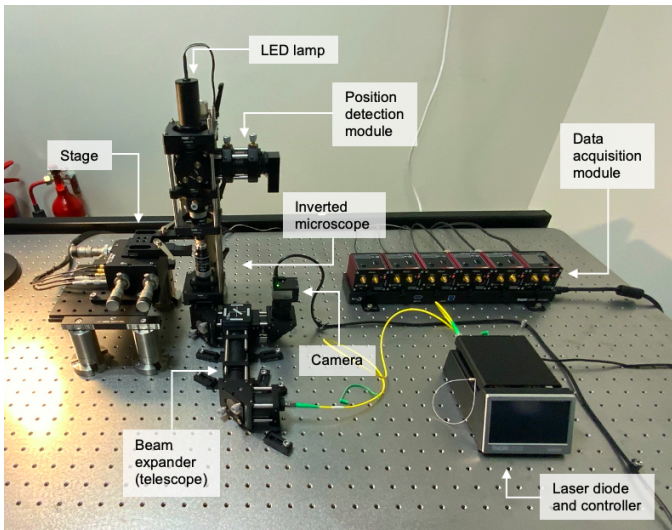


Figure 2: A photo of the instrumental setup with the main parts labeled. An optical trap has two light sources: a laser to trap a particle and an LED lamp to visualize the sample. A camera provides the image of the sample. The position of the bead is recorded with a QPD in the position detection module. The optical setup consists of a telescope as a beam expander and an inverted microscope as a trapping apparatus. Data from the QPD and the strain gauges in the stage is collected using the K-Cube data acquisition module.

*Detailed schematic of optical setup.* We will now explain the optical setup of OT by following the path of the laser, as shown on Fig. 3. For more details on the setup, please refer to the Thorlabs user guide [11, 12] or webpage [10].

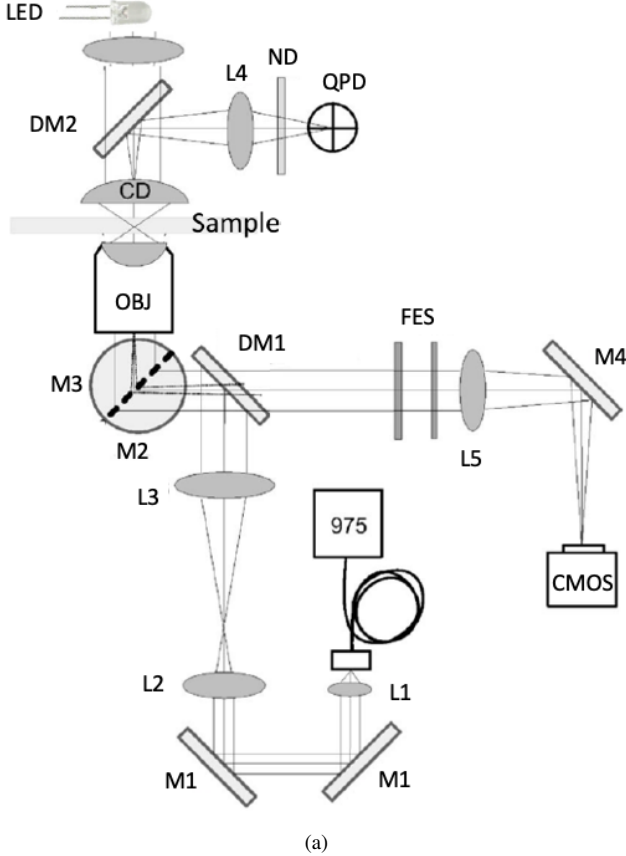
1. **Laser source.** A near-infrared laser of wavelength 976 nm was used. The laser diode is enclosed and is coupled with a TEC controller which maintains its temperature at 25°C to ensure a stable power output. The TEC is coupled with the feedback loop from a temperature sensor, and accordingly regulates the current output to the thermoelectric module that controls the diode temperature. This is necessary in order to apply a stable force on the trapped particle. The controller allows to change the laser power by setting the current through the diode between 0 – 400 mA. The laser

beam is then channeled through an optical fiber and is collimated with a triplet lens upon entering the optical setup (L1 on Fig. 3a). At this point the beam diameter is expected to be 1.7 mm.

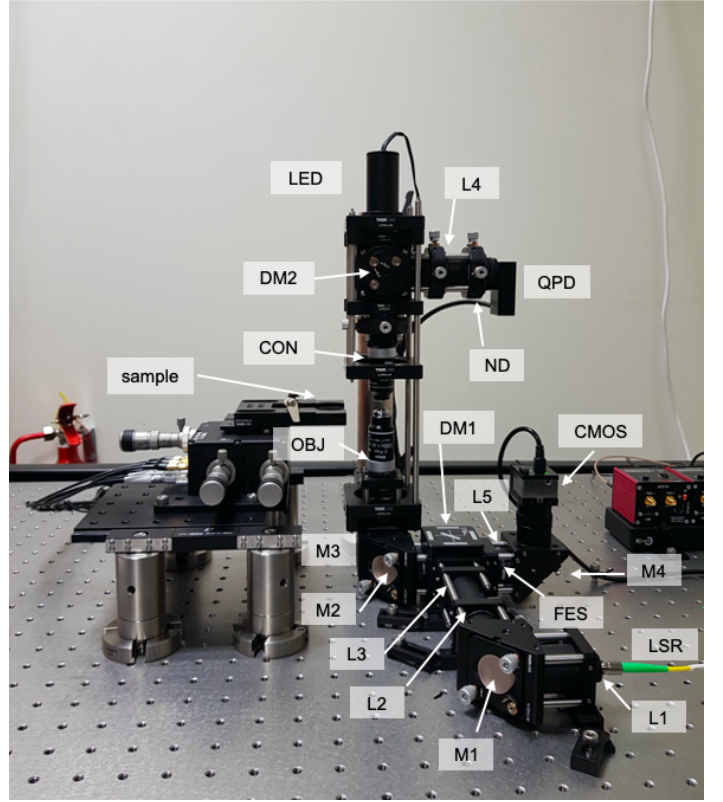
2. **Beam expander (telescope).** In order to match the size of the objective, the beam is expanded with a Galilean beam expander. Before the expander, a turning mirror (M1) directs the laser and is used to center the beam. An achromatic doublet of a converging (L2,  $f = 150\text{ mm}$ ) and a diverging (L3,  $f = -50\text{ mm}$ ) lens is used to increase the beam diameter to about 5 mm. When fully assembled the distance between the two lens is fixed by the manufacturer to ensure the beam is collimated after the beam expander. To adjust this distance it is necessary to disassemble the beam expander section and manually place the lens at a desired distance.
3. **Dichroic filter cube.** Next the laser beam passes through a dichroic mirror (DM1) which reflects only infrared light and lets visible light pass through. That is, the mirror reflects the laser beam towards the objective and lets the light from the LED pass towards the camera. After this the beam passes through an iris and two steering mirrors (M2, M3), and proceeds vertically towards the objective. The two mirrors can be adjusted to center the beam.

4. **Inverted microscope.** The beam is then focused on the sample with a 100X oil immersion objective lens (OBJ, numerical aperture 1.25, working distance 0.23 mm). Each time a sample is to be observed, a drop of oil needs to be placed on the objective. Oil with a refractive index higher than air and similar to the material (glass) of the focusing lens is used to increase the numerical aperture of the objective. This means that the type of oil is specific to the objective lens, but because oil was not provided with the kit we used the one provided by Professor George Shubeita (from a different objective). The usage of oil improves the magnification of the image of the sample and reduces the waist of the laser trap. The oil needs to be applied each time a sample is placed on the stage to be looked at with the microscope. The diameter of the focused beam is expected to be 1.1  $\mu\text{m}$ . The scattered laser light is then collected with a 10x air condenser lens (CON, numerical aperture 0.25, working distance 7 mm). The vertical position of the condenser is easily adjustable and was set such that the laser beam is collimated after the condenser (around 7 – 8 mm). In the beginning (data set 1 and 2 at [13]) we used the objective lens provided with the setup. After troubleshooting (see section 3.1.2) we borrowed a similar one from Prof. Shubeita's lab: a 100x oil immersion objective of numerical aperture 1.3 [14], which was recommended by Thorlabs for usage with silica beads. All the data presented in this report was taken with this new objective lens.

5. **Position detection module.** The laser light scattered off the bead leaves the condenser and is reflected off a dichroic mirror (DM2). Before reaching the QPD it is focused with a converging lens (L4,  $f = 40\text{ mm}$ ) and passed through a neutral-density filter (ND) to minimize QPD saturation. These two elements can be adjusted to center the beam on



(a)



(b)

Figure 3: Schematic and photo of the optical setup. Schematic (a) is a modified version of Fig. 1 in reference [15]. Legend: L - lens, M - mirror, DM - dichroic mirror, OBJ - objective, CD/CON - condenser, ND - neutral-density filter, QPD - quadrant photodiode, LSR - laser, FES - shortpass filter, CMOS - camera. The setup is described in detail in section 3.1.1.

the QPD screen. The laser needs to be centered every time the optical trap is used. The QPD consists of four optically active areas (quadrants) that together form a circle of diameter 7.8 mm (see Fig. 4). Each section produces an electric signal with current proportional to the intensity of the incoming light. The embedded circuit in the QPD computes a voltage for each coordinate in 3D that corresponds to the position of the bead along that coordinate relative to the center of the trap. The circuit assumes a positive x-axis is towards left (9), positive y-axis is towards up (10) and positive z-axis represents an increase in total light intensity reaching the QPD (11).

$$V_x = (Q_2 + Q_3) - (Q_1 + Q_4) \quad (9)$$

$$V_y = (Q_1 + Q_2) - (Q_3 + Q_4) \quad (10)$$

$$V_z = (Q_1 + Q_2 + Q_3 + Q_4) \quad (11)$$

6. **Stage.** The stage allows to move the sample in three directions - X, Y, Z. The position can be changed manually and electrically. Manually: the stage can be pushed, the sample can be moved around, or the differential micrometers can be used for precise adjustments with resolution of 5  $\mu\text{m}$  (coarse adjusters) or 0.5  $\mu\text{m}$  (fine adjusters). Electrically: the piezoelectric actuator motors built in the stage

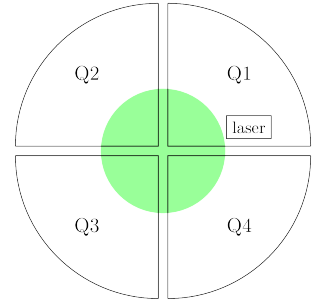


Figure 4: A diagram of the four optically active areas of the QPD. Each area produces a signal with current proportional to the light reaching that area.

can be used to move the stage very precisely for up to 20  $\mu\text{m}$  in total, in a controlled manner and with high frequency. To produce the movement, a voltage controller (the K-cube Piezo Controller) applies high voltage on a piezo material. The voltage controller can be used in open loop mode, or in closed loop mode using feedback from the strain gauge readers in the stage. The position of the sample can be inferred using the scale on the micrometers or the voltage output from the strain gauges, read with the Strain Gauge K-cube.

**7. LED and camera module.** Light from the LED lamp is focused on the sample with the condenser (bright-field illumination) and then collected with the objective. The light then passes through the dichroic mirror (DM1) towards the CMOS camera. Before reaching the camera, it passes through a bandpass filter (FES) that prevents any laser light (for example, backscattered off the slide and passing through the dichroic mirror) from reaching the camera, and is focused with an achromatic doublet lens (L5). We eventually removed the bandpass filter in order to be able to see the backscattered laser on the camera view. The laser is visible when the microscope is focused on the coverslip or slide surface, but the image at the coverslip was stronger and was used as a reference of the position of the laser beam.

*Data acquisition module.* As pictured on Fig. 5 the output information we get from the system is:

- A photo of the sample, obtained with the CMOS camera. The camera is connected to a computer and the output can be accessed in real time using the ThorCam software.
- Relative position of the bead in the trap obtained with the QPD in the form of voltage output for each of the three axis:  $V_x$ ,  $V_y$  and  $V_z$ . The QPD output is connected to a K-Cube Position Aligner which displays the position of the laser on the QPD surface and computes the output voltage for each axis. The voltages are sent to a computer via a Multifunction Input/Output (I/O) Controller and are processed in LabVIEW. The LabVIEW application plots the following: voltage vs time graphs, power density spectra and potential for each axis. Raw data can be exported using the *Log and Save* option in the Logging Settings feature (see Fig. 6a) or by right-clicking on the voltage vs time graphs and choosing the export option.
- The strain gauge output is read by the K-Cube Strain Gauge Readers and is displayed in terms of force, position or voltage. It can be read from the K-cube screen or via the Kinesis software by connecting the K-Cube holder (controller hub) to a computer. There are two cube readers which can be arranged to show any two axis of interest. We used X and Y, or X and Z at different parts of the experiment. It is possible to use these readers to read the position of the stage, but we decided not to use them that way because we observed a difference between the position change measured with the K-cube reader and the distance that a fixed bead in the sample moved on the camera screen expressed in terms of bead diameter - indicative of incorrect conversion from voltage to position. Therefore, the purpose of the strain gauge readers in our experiment was to enable closed-loop operation of the piezo controllers and redirect the strain gauge voltage signal towards the I/O controller.

In turn we can control the position of the stage with the K-cube Piezo Controller using the following methods:

- Choosing the appropriate settings and manually changing

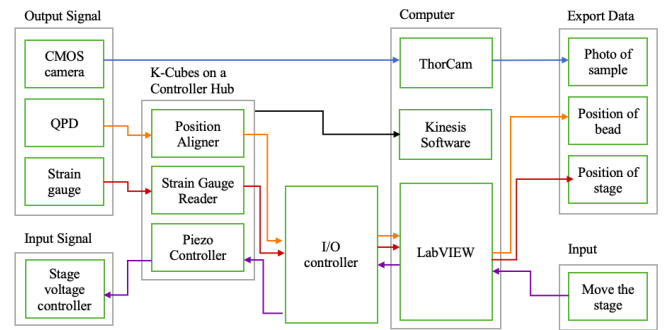


Figure 5: A diagram showing how data is handled. The camera signal is directly read with a computer using ThorCam. The QPD and strain guage signals are processed with a K-cube and read from the cube, the Kinesis software on a computer or in LabVIEW via the I/O Controller. The stage is moved by controlling the signal from the K-cube piezo controller via LabVIEW.

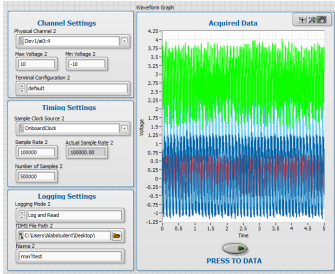
the voltage on the physical K-cube interface or in the Kinesis software on a computer.

- Use the options in the LabVIEW application (see Fig. 6c) to send a voltage-controlling signal to the K-cube controller via the I/O controller. Specifically, the interface we designed in LabVIEW allows to send discrete pulses or continuous waves of different shape (triangular, rectangular, sinusoidal), frequency, amplitude and choose the offset and phase.

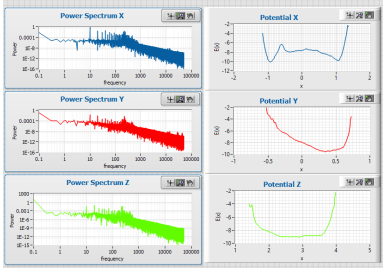
*Alignment procedure* During the assembly of the instrument we performed a laser alignment procedure. With an IR viewing card we checked if the laser is collimated as expected: after the initial collimator (L1), after the beam expanding section (L3), just before the objective and after the condenser. We centered the laser beam using an IR alignment disk [16] at the following locations: after the first mirror (M1) and the beam expander (L3) by adjusting M1, after the second mirror (M2) by adjusting M1 and M2, after the third mirror (M3) and after the condenser by adjusting M1-3, and after the dichroic mirror (DM2) by turning DM2. The adjustment after M3 was done by performing a standard two-point alignment procedure using the iris between M2 and DM1, and the iris between M3 and OBJ. That is, the laser was adjusted to ensure maximum laser throughput of each iris separately and when both irises are closed. We repeated this alignment several times during the assembly. The last alignment was done on February 8th. Note that on February 10th and 13th we moved around the lens in the beam expanding region in attempt to bring the focus of the laser closer to the focal point of the objective (see Section 3.1.2). Although we placed back the two lens in their previous position, it is possible that small disruptions in alignment were made as a result. Based on previous experience with the alignment we didn't expect these to be significant so we proceeded without redoing the alignment.

### 3.1.2. Troubleshooting

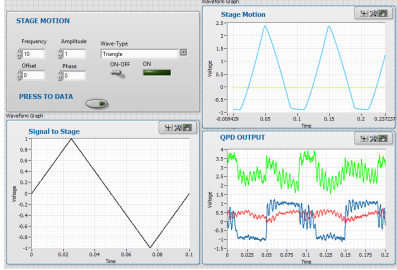
A shortcoming of the apparatus that took a significant amount of time to uncover was that the focal point of the objective did not coincide with the focus of the trap. As a result when a bead is fixed at the center of the trap, it appears to be



(a) Interface for obtaining data.



(b) Interface displaying the power spectrum and potential, computed from raw data.



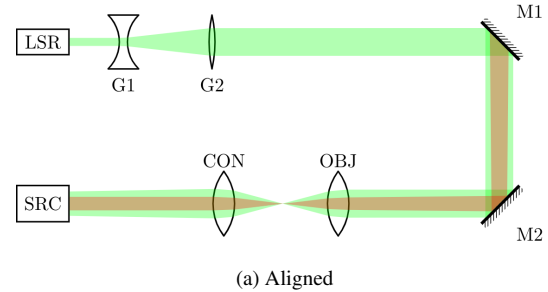
(c) Interface for moving the stage and plotting relevant data.

Figure 6: A screenshot of the LabVIEW application we used. We were initially provided with an application that contained many of the features seen in (a) and (b). We modified and reorganized it to fit the needs of our experiment - the version shown here.

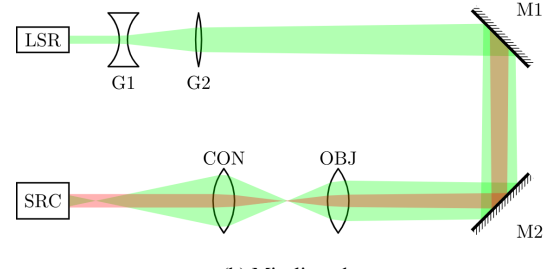
out of focus relative to the camera. The reason for such a misalignment is shown in Fig. 7b.

Fig. 7 shows a simplified version of the optical trap setup described in section 3.1.1. Specifically we have isolated the setup to two main components: the Galilean beam expander, and the objective-condenser setup. Everything that we see in focus from the camera is what lies on the focal point of the objective. When everything is aligned perfectly (see Fig. 7a) the laser light from the beam expander is collimated when it reaches the objective. Then, the laser is focused exactly at the focal point of the objective which translated to seeing the trapped object in focus. However, we believe that in our setup the Galilean beam expander was not aligned properly (as seen in Fig. 7b) resulting in the laser light not being collimated upon reaching the objective. As a result, the laser was focused in before the objective's focal point.

To figure out whether or not the laser was focused in front of the objective's focal plane or after, we followed the procedure



(a) Aligned



(b) Misaligned

Figure 7: Simplified schematic of the optical setup for the trap. LSR is the trap laser beam, G1 and G2 the mirrors of the Galilean telescope, M1 and M2 the adjustable mirrors, OBJ the objective lens, CON the condenser lens, and SRC the white light source. The green rays represent the laser emanating from LSR, while the red rays emanate from SRC. (a) shows a setup that is perfectly aligned, i.e. the focal point of the objective overlaps with the focus of the trap light. (b) shows a misaligned setup, where G2 has moved which results in the trap light being focused before the objective's focal point.

outlined below.

1. Remove the IR filter in front the camera (see section 3.1.1). This way we would be able to see the reflection of the laser from the coverslip.
2. Focus on the interface between the coverslip and the water. We can do that by finding specs that are stuck at the boundary.
3. Move the stage up and down until the reflection of the trap's laser is visible on the camera.

We focused on the boundary between the water and the coverslip, because this is where the refractive index would change in our setup. Since we are using an oil immersion objective (see section 3.1.1) the difference in the index of refraction in the oil-coverslip boundary is almost 0, while it is much bigger in the coverslip-water boundary. From (12) we know that the difference in index of refraction is proportional to the reflectivity of a boundary [17].

$$R = \left| \frac{n_1 - n_2}{n_1 + n_2} \right|^2 \quad (12)$$

where  $n_i$  is the index of refraction of medium  $i$ , and  $R$  is the reflectivity of their boundary. In our case the refractive index of the coverslip glass was  $n_{\text{glass}} = 1.517$  [18], the refractive index of the immersion oil was  $n_{\text{oil}} = 1.518$  [14], and the refractive index of water is known to be  $n_{\text{water}} = 1.333$ . Hence,

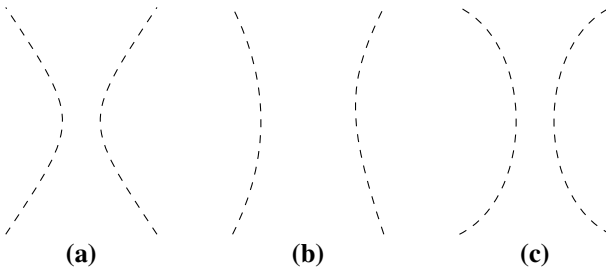


Figure 8: Side view of multiple configurations for the spherical aberration of the focal point. (a) shows a perfectly focused trap in both X, Y, and Z, (b) shows an unfocused trap that suffers from aberration in all directions, while (c) shows a trap that is focused on the X-Y plane, but unfocused on the Z-plane.

we can calculate the reflectivity of the oil-coverslip boundary to be:  $R_{oc} = 1.09 \times 10^{-7}$  while for the coverslip-water boundary:  $R_{cw} = 4.21 \times 10^{-3}$ .

### 3.1.3. Current operation mode

The main issue observed with the apparatus was the lack of sufficient trapping efficiency on the Z axis. Specifically, when trapping a bead we noted that moving the stage in the Z-direction would change the focus of the bead. This behaviour is unexpected because if the bead was trapped in the Z axis the motion of the stage would leave it unaffected, therefore the relative distance between the center of the trap and the focal point of the objective would remain constant, resulting in a bead that does not change focus under such a motion. Our observations suggested that the bead was in fact moving in the z-axis along with the stage.

This suggests that the drag force from the surrounding water was strong enough to push the bead along this axis at any position. Our current hypothesis as to how this could occur is that there is significant spherical aberration along the Z-axis leading to many stable points where the potential is minimum. To illustrate this point consider the sketch in Fig. 8. We believe that the focused trap beam looks like part (c) of this figure where the aberration on Z is high enough to create a long stem of multiple stable equilibrium positions, while still having high trapping efficiency in Z.

Therefore the question of calibration arises. Since we do not know at what position in z we are in, it becomes entirely possible that we have trapped a beam close to the cover slip. If the bead is close enough the drag force due to shear viscosity is high with respect to the Brownian motion of the bead. In this case we would obtain false readings for our calculated quantities throughout the experiment such as Boltzmann's constant and trap stiffness. As a result we have devised the following calibration procedure, illustrated below.

1. Trap a bead
2. Move the stage in a sawtooth manner along X or Y with frequency 10 Hz and an amplitude of  $4 - 6 \mu\text{m}$  for 5 seconds.
3. Record position data with the QPD. A sample of such data, along multiple Z positions, is shown in Fig. 9.

4. If no mixing is seen along the coordinates (i.e. the QPD signal looks flat during the rising phase) then the Z-position is high enough that shear viscosity does not have a significant effect in the motion of the bead.

5. Otherwise change the Z-value and repeat,

In essence, with this procedure we move the bead very fast from point to point to examine the drag forces applied to it. If the bead is close to the cover slip then the shear viscosity as seen in (13) (an equation from FoS 1-2) will increase. Increasing the drag force from viscosity will introduce some additional impedance to the motion of the bead, thus the rough change of the sawtooth signal will be detected by the QPD during the ramping phase, as we see in Fig. 9. Otherwise if we are at an appropriate height, the impedance will be almost 0, hence the signal will look straight during the ramping phase.

$$P_\eta = \eta \frac{dv_x}{dz} \quad (13)$$

where  $\eta$  is the coefficient of shear viscosity,  $v_x$  is the velocity parallel to the coverslip,  $z$  is the distance from the coverslip, and  $P_\eta$  is the pressure due to the viscosity.

### 3.2. Calibration procedure

There are three unknown quantities needed in order to use the instrument for measuring forces: (1)  $\rho$  (units: m/V), the displacement sensitivity of the QPD to convert the voltage signal from the QPD into position units; (2)  $k_{trap}$  (units: N/m), the stiffness of the optical trap to convert position data into forces; and (3)  $\gamma$  (units: kg/s), the drag coefficient of the bead to accurately calculate the drag force and compare between different methods for measuring the trap stiffness [19]. In this section we describe the theory and procedure behind each calibration process. A more detailed step-by-step description of the procedure can be found in [Appendix A](#).

#### 3.2.1. Stage and QPD Calibration

*Theory* The time-series that a QPD provides is the main source of precise data about the position of the bead in the trap, so an accurate calibration is essential for using the instrument. To find the displacement sensitivity we move a stuck bead across the laser trap for a known distance and relate that to the voltage signal of the QPD [20, 21]. To determine the physical distance the bead moves we can use the stage position or the camera output. We used the stage because the strain gauges provide a precise measure of position. The following quantities need to be found:

- The stage position-voltage conversion factor  $\beta$ , where  $\Delta r = \beta \Delta V_{stage}$ .
- The QPD-stage voltage conversion factor  $\alpha$ , where  $\Delta V_{stage} = \alpha \Delta V_{QPD}$ .

*Procedure* To find the stage position-voltage factor  $\beta$ , we moved the stage by sending a single voltage pulse with defined amplitude through LabVIEW. We then used the differential micrometers to find the distance the stage moved. We repeated this for several voltage values, separately for X and Y axis, and

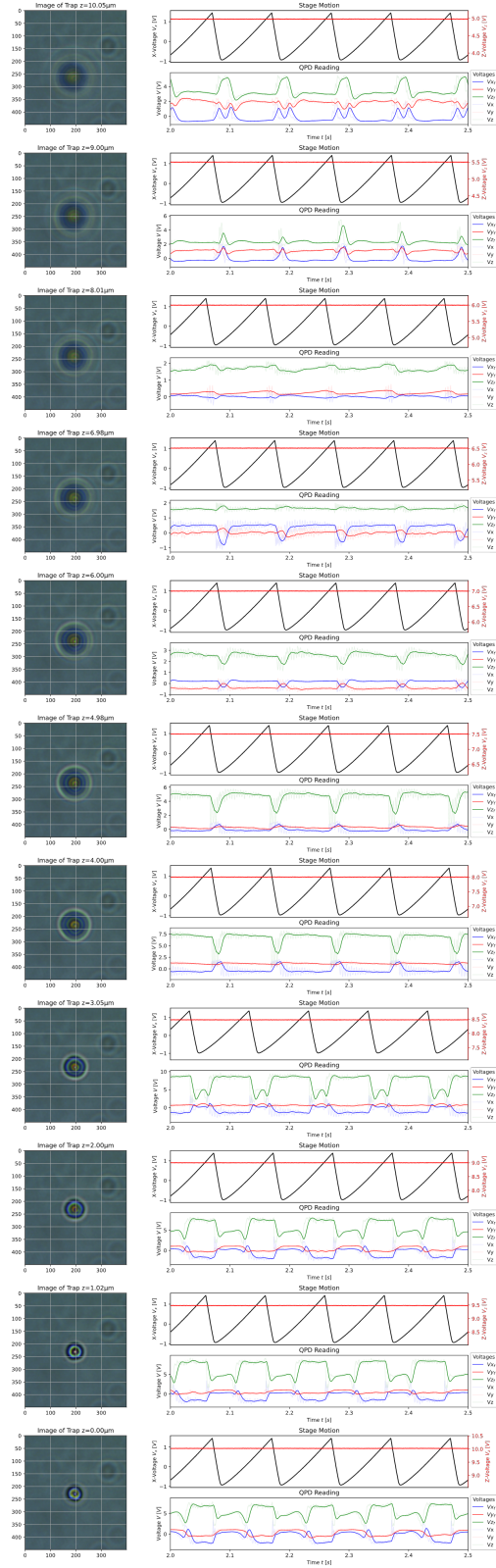


Figure 9: The effect of a sawtooth signal on the x axis of the stage to the QPD reading at multiple z positions. Each row represents a different z-position from the cover slip starting from  $0 \mu\text{m}$  (bottom) to  $10.05 \mu\text{m}$  (top). On the left of each row there is a picture of the trapped bead. On the top right of each row there is the position data from the strain gauge sensor for the stage as a function of time, while in the bottom right the filtered QPD data are presented as a function of time. A higher resolution version of this image can be found [here](#)

linearly fitted the position vs voltage data. The slope of this graph is the factor  $\beta$ .

To find the QPD-stage voltage conversion factor  $\alpha$ , we drove the stage with a triangular wave of frequency  $10 \text{ Hz}$  and amplitude  $2 \mu\text{m}$  for 5 seconds and recorded the QPD and strain gauge data. We used a solution of silica beads (diameter  $2 \mu\text{m}$ ) in PBS with  $1:10k$  dilution. We repeated this at several laser powers, separately for X and Y axis which fixed the beads to the two surfaces. The QPD voltage is linearly related to the position of the bead in the trap only within a certain range. Then, we are interested in the part of the data generated with this movement where the voltage changes linearly in time. Once we have selected the portion of the data that is of interest, we plot the QPD voltage vs strain gauge voltage. The slope of the best linear fit gives the factor  $\alpha$ .

### 3.2.2. Optical Trap Calibration

**Theory** To find the trap stiffness and drag coefficient we used three methods, all of which take advantage of quantities that characterize the motion of a bead in the trap potential. A trapped bead is essentially a harmonic oscillator in a fluid and can be described with Langevin's equation. That is, the bead experiences the following forces (equation (14)): a restoring linear force of the laser beam,  $-k_{trap}x$ ; a Stokes' drag force from the collisions with other particles in the solution,  $\gamma\dot{x}$ , where  $\gamma = 3\pi\eta d$  is the drag coefficient,  $d$  is the diameter of the bead and  $\eta$  is the viscosity of the fluid; and a random force from these collisions due to the purely random thermal fluctuations,  $F(t)$  [22, 21]. As this is the low Reynolds' number regime, the inertia is negligible compared to the drag force so the equation can be approximated to equation (15) [21].

$$m\ddot{x} = -k_{trap}x - \gamma\dot{x} + F(t) \quad (14)$$

$$\gamma\dot{x} + k_{trap}x = F(t) \quad (15)$$

After collecting time-series data for the position of a trapped particle, we looked at the following quantities:

1. **PSD.** Using the time series data we can construct a power spectrum distribution (PSD) as defined with the Wiener-Kinchin theorem [21]. That is, the PSD is the Fourier Transform of the average value of the autocorrelation function. This means the PSD is:

$$S_{xx}(f) = \sqrt{\frac{k_B T}{\pi^2 \gamma (f^2 + f_0^2)}} \quad (16)$$

where  $f_0 = \frac{k_{trap}}{2\pi\gamma}$  is the corner frequency of the spectrum. This can be derived by taking the Fourier transform of the equation of motion (15) and using that the power spectrum of  $F(t)$  (white noise) is  $\sqrt{(4\gamma k_B T)}$ .

2. **Potential energy.** From Boltzmann distribution, we know that the probability to find the bead in a particular energy "level" of the trap potential is proportional to the Boltzmann factor  $\exp(-\frac{U(x)}{k_B T})$ . We use (17) to construct a histogram of the potential energy which we then fit with the expected quadratic potential of the trap (18).

$$U(x) = -k_B T \ln \left( \frac{P(x)}{P_0} \right) \quad (17)$$

$$U(x) = \frac{1}{2} k_{trap} x^2 \quad (18)$$

3. *Equipartition theorem.* By the equipartition theorem, it follows that the total energy of the system (assumed to be at thermal equilibrium  $T$ ) for each degree of freedom is equal to  $k_B T/2$ , where  $k_B$  is the Boltzmann's constant and  $T$  is the temperature. As a particle in harmonic potential, the average energy of the bead along each coordinate is  $k_{trap} \langle x^2 \rangle / 2$ , where  $\langle x^2 \rangle$  is the variance of the position in one coordinate i.e. recorded time series. This allows us to find the trap stiffness by using the time series to calculate the variance (equation (19)).

$$\frac{1}{2} k_{trap} \langle x^2 \rangle = \frac{1}{2} k_B T \quad (19)$$

*Procedure* The only data needed for this calibration is the time series of a trapped bead, as recorded with the QPD. The step-by-step procedure used for this can be found in [Appendix A](#). Then, we find the trap stiffness with each of the three methods described above: (1) by computing and fitting the power spectrum; (2) by constructing the energy histogram and fitting it; (3) by computing the variance, using equipartition theorem. We also extract a value for Boltzmann's constant and drag coefficient from the fits to the PSD/

## 4. Results

### 4.1. Stage and QPD Calibration

In this section we present the data obtained from calibrating the stage by applying a known voltage and measuring the distance travelled along each axis, as well as the QPD output obtained by moving a  $2\mu m$  bead across the trap. The aim of this section is to establish the conversion factors between the voltage output of the QPD and gauge readers to the actual distance measured in  $\mu m$ .

We begin by presenting the data for the distance moved by the stage as a function of the voltage applied to its piezoactuators. The methodology for obtaining such data can be found in section [3.2.1](#) and the raw data along with the analysis code can be found [here](#). Fig. 10 illustrates this data. The numerical values for the conversion factor between applied voltage and change in position  $\beta_x$  and  $\beta_y$  for X and Y axis respectively is shown with errors in Table 1. We will be using these conversion factors to account for the change in the distance of the stage and calculate the rest of the quantities.

Moving on, as per the methodology described in section [3.2.1](#) we have obtained the voltage output of the QPD as a response of moving a  $2\mu m$  bead across the trap in both the X and Y axes. The raw data, as well as the analysis code can be found [here](#).

As described in section [3.2.1](#) in order to obtain the proper calibration coefficients we need to identify the region of the bead's motion during which it is moving at constant rate through the trap. We did so, by considering the following procedure.

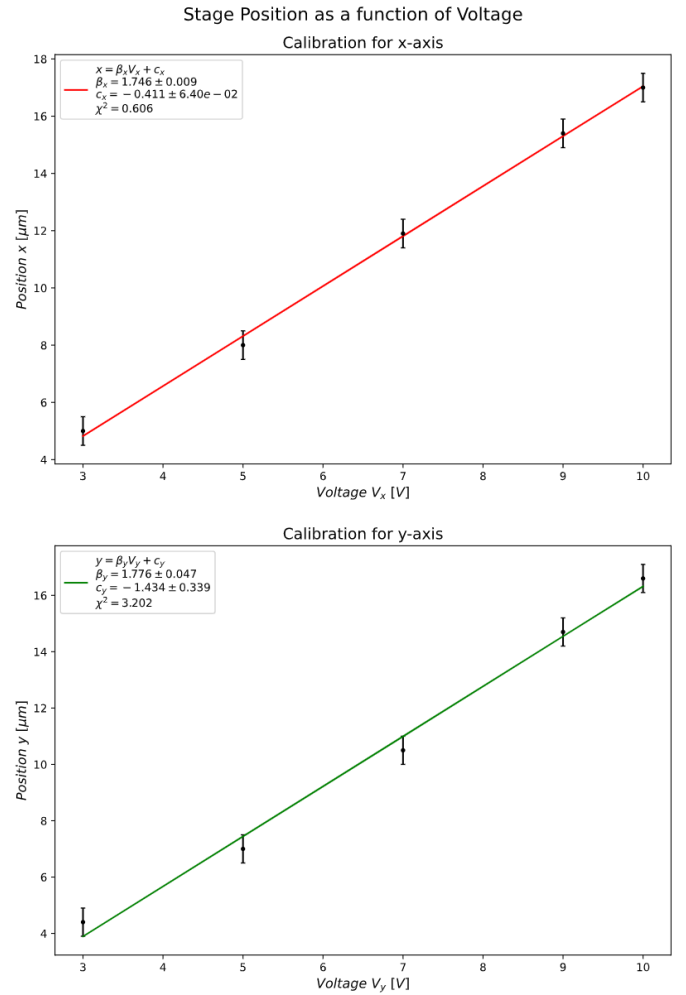


Figure 10: Stage position as a function of voltage. A set voltage was applied incrementally to the stage and the recorded change in position is shown in the plot above for motion in the x-axis (red) and in the y-axis (green). The fit parameters for each best fit line are also displayed in the legend.

1. Filter the data using a Butterworth Low Pass filter of the first order, to cutoff every frequency above  $f_c = 100 Hz$ . The filter's transfer function is shown in (20).

$$H(i\omega) = \left( 1 + \varepsilon^2 \left( \frac{\omega}{\omega_0} \right)^{2n} \right)^{-1/2} \quad (20)$$

where  $\omega$  is the frequency,  $\omega_0$  is the cutoff frequency,  $n$  is the order of the filter, and  $\varepsilon$  is the gain at  $\omega = 0$ .

2. After removing the thermal noise of all the data sets, the

Variable	Value	Error	Unit
$\beta_x$	1.746	$\pm 0.009$	$\mu m/V$
$\beta_y$	1.780	$\pm 0.050$	$\mu m/V$

Table 1: Conversion factors assuming the relationship between stage driving voltage and position to be of the form  $\Delta x_i = \beta_i \Delta V_i$ .

derivative was calculated pointwise by the simple first order Euler approach (see in (21)).

$$\frac{\partial A}{\partial t} \Big|_t \approx \frac{A(t + \Delta t) - A(t)}{\Delta t} = f_s(A(t + \Delta t) - A(t)) \quad (21)$$

where  $f_s$  is the sampling frequency.

3. With the new signal identified we wrote an algorithm to select the regions where the derivative was flat (the code can be found [here](#)).
4. Finally we obtained the stage voltage and QPD voltage for each region and plotted the first vs the latter. We fit each curve of the family of curves so as to obtain a statistical estimate of the standard deviation of the slope and intercept.

Variable	Intensity	Value and Error [ $10^{-2}\mu\text{m}/V$ ]
$\alpha_x$	100 mA	$15.9 \pm 0.20$
	150 mA	$8.50 \pm 0.10$
	200 mA	$5.61 \pm 0.08$
	250 mA	$4.49 \pm 0.05$
	300 mA	$3.66 \pm 0.05$
	100 mA	$17.4 \pm 0.20$
	150 mA	$9.70 \pm 0.10$
	200 mA	$5.02 \pm 0.07$
	250 mA	$3.91 \pm 0.04$
	300 mA	$3.35 \pm 0.03$

Table 2: Conversion factors assuming the relationship between stage driving voltage and position to be of the form  $\Delta x_i = \beta_i \Delta V_i$ .

This method was carried out for all the intensities in order to obtain the conversion coefficients listed in Table 2. The full plots are too distracting to place in the main text, hence they are included in [Appendix B](#). However we have included a sample plot for an intensity of 100mA in Fig. 11.

Putting the two conversion factors together, we finally get the displacement sensitivity  $\rho$  for each laser power, separately for X and Y. The values are given in Table 3 and were used in Section 4.2 to convert the QPD voltage into position data.

#### 4.2. Trapped bead calibration

In this section we present the values of the trap stiffness, drag coefficient and Boltzmann's constant found using the three methods described in Section 3.2.2. The values were calculated separately for X and Y. We omitted an analysis of the Brownian motion in the Z direction because we had previously observed that the bead is not fully trapped in Z, so the obtained data may be specific to the neighbourhood of the position at which the bead was trapped and cannot be generalized.

The methodology for obtaining the trapped bead data can be found in Section 3.2.2 and the raw data and data analysis can be found [here](#).

Variable	Intensity	Value and Error [ $10^{-2}\mu\text{m}/V$ ]
$\rho_x$	100 mA	$27.8 \pm 0.10$
	150 mA	$14.76 \pm 0.08$
	200 mA	$9.80 \pm 0.05$
	250 mA	$7.84 \pm 0.04$
	300 mA	$6.40 \pm 0.03$
	100 mA	$30.8 \pm 0.8$
	150 mA	$17.2 \pm 0.5$
	200 mA	$8.9 \pm 0.2$
	250 mA	$6.9 \pm 0.2$
	300 mA	$5.9 \pm 0.2$

Table 3: Displacement sensitivity of the QPD, used to convert the voltage data into position. Obtained from the two conversion factors as  $\rho_i = \alpha_i \beta_i$ .

As discussed in Section 3.2.2, to find the trap stiffness we need to compute the PSD, energy histogram and variance of the position time series. In order to generate the power spectrum and energy histogram, the following procedure was followed:

1. The QPD voltage data for each axis - X and Y - was centered around zero by finding the average value and subtracting it from each data point. This is needed in order to use the calibration factor  $\rho$  found in Section 4.1 which relates a change in voltage with a change in position, and so that the potential energy histogram is centered around 0 in X and Y. Then the position data was generated as follows:

$$r_i = \rho_r(V_{ri} - \bar{V}_r) \quad (22)$$

where  $r$  is the position coordinate,  $i$  is the data point,  $\rho_r$  is the appropriate displacement sensitivity and  $V$  is the voltage.

2. We computed the square of equation (16) from the position time-series. A power spectrum can be estimated as the square of the Fourier transform of a time-series. We computed the PSD with the Periodogram function (using 'density' scaling) of the Signal Processing submodule in the SciPy package. This function uses the Welch's method of estimating PSD, that is it divides the data into overlapping windows, finds the periodogram (square of Fourier transform) for each window and then finds the average of all computed power spectra [23]:

$$S_x^W = \frac{1}{K} \sum_{k=1}^K \frac{1}{M} |FT(f)|^2 \quad (23)$$

where K is the number of windows, M is the number of data points in a window.

3. In order to improve the fits, the PSD was rescaled and a moving average was found. The rescaling was done such that the data points are evenly spread along the x-axis of a log-log plot. The window length of the moving average was chosen to be 0.005 of the length of the rescaled PSD data set.

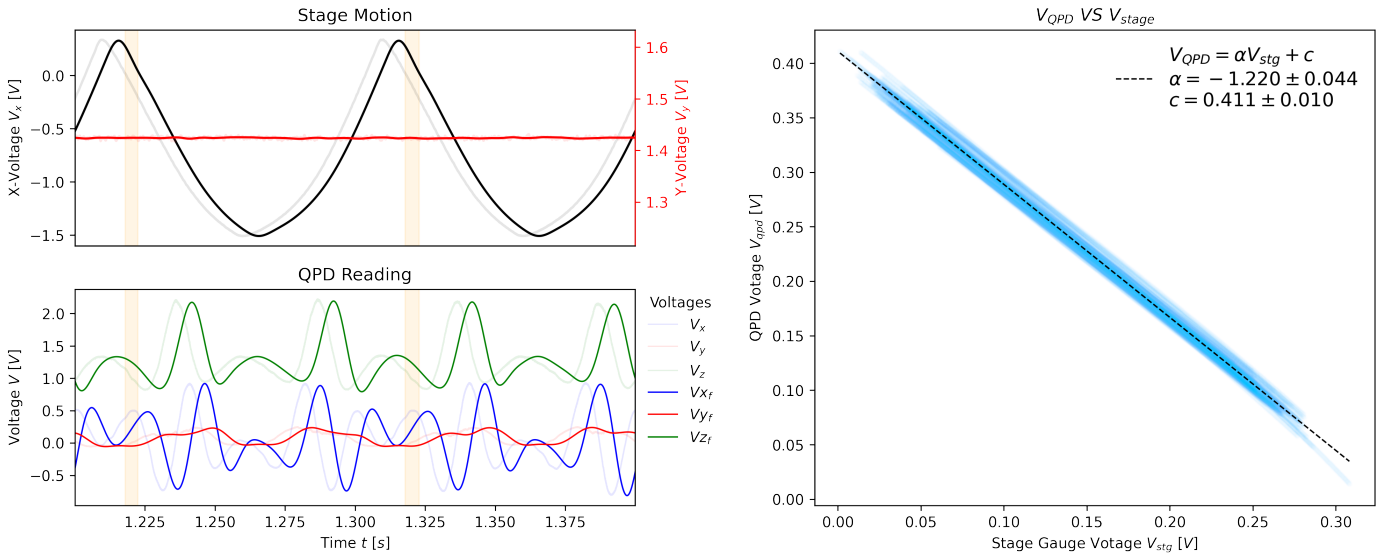


Figure 11: Voltage of Stage  $V_{stg}$  VS Voltage of QPD  $V_{QPD}$  for a stuck,  $2 \mu\text{m}$  bead across the trap beam. In the left side plots solid lines represent the filtered signal, while transparent lines represent the original signal. The orange highlighted regions are the ones identified by the algorithm as having a linear relationship in both the stage and the X-signal of the QPD (blue curve). The top left side shows the motion of the stage, while the bottom left the output of the QPD. On the right with transparent blue is the superposition of all the  $V_{stg}$  VS  $V_{QPD}$  plots identified throughout the 5s signal. With dashed solid blue is the average fit of all such curves. The reader is encouraged to look at [Appendix B](#) for the complete plot.

4. The potential energy was found by constructing a histogram of the position data, representative of the probability of the bead to be found at each position ( $P(x)/P_0$ ) and then calculating equation (17).

As described in Section 3.2.2, the trap stiffness was found from each of the three approaches: power spectrum density, potential energy and equipartition theorem.

The final PSD was fit with function (24) which has two free parameters: the coefficient  $A$  (25) and the corner frequency  $f_0$  (26). Using the known value of the Boltzmann's constant ( $1.38 \times 10^{-23} \text{ J/K}$ ), an experimental value of the drag coefficient was found from the coefficient  $A$ , using equation (25) and assuming room temperature of 298.15 K. The experimental value of the trap stiffness was calculated from the fit parameter  $f_0$  and the experimental drag coefficient, using equation (26). On the other hand, by assuming a theoretical value of the drag coefficient using a literature value of the viscosity of water ( $\eta = 8.9 \times 10^{-4} \text{ Pa} \cdot \text{s}$ ,  $d = 2\mu\text{m}$ ,  $\gamma = 1.68 \times 10^{-8} \text{ kg/s}$ ), we calculated the Boltzmann's constant experimentally using equation (27).

$$S_x^W = \frac{A}{f^2 + f_0^2} \quad (24)$$

$$A = \frac{k_B T}{\pi^2 \gamma} \quad (25)$$

$$f_0 = \frac{k_{trap}}{2\pi\gamma} \quad (26)$$

$$k_B = \frac{3\pi^3 \eta d}{T} A \quad (27)$$

Next, the trap stiffness for each axis and laser power was

found in the other two ways: as a parameter for the parabola fitting the potential energy histogram; and using the equipartition theorem by calculating the variance of the position time-series and plugging it in equation (19).

The values of the trap stiffness obtained with the three different methods are presented in Table 5. The values of drag coefficient and Boltzmann's constant derived from the fit parameter  $A$  are presented in Table 4. The figures for each laser power are provided in [Appendix D](#). As an example, please refer to Fig. 12 for how the PSD and potential energy graph and fit look like.

Axis	Intensity	Drag $\gamma$ [ $10^{-8} \text{ kg/s}$ ]	$k_B$ [ $10^{-23} \text{ J/K}$ ]
X	100 mA	$8.4 \pm 0.3$	$0.276 \pm 0.009$
	150 mA	$8.2 \pm 0.3$	$0.28 \pm 0.01$
	200 mA	$10.2 \pm 0.4$	$0.23 \pm 0.01$
	250 mA	$9.1 \pm 0.5$	$0.25 \pm 0.01$
	300 mA	$8.1 \pm 0.4$	$0.29 \pm 0.01$
Y	100 mA	$124 \pm 3$	$0.0187 \pm 0.0005$
	150 mA	$44 \pm 2$	$0.0530 \pm 0.0020$
	200 mA	$133 \pm 1$	$0.0174 \pm 0.0002$
	250 mA	$127 \pm 1$	$0.0183 \pm 0.0002$
	300 mA	$102.9 \pm 0.9$	$0.0225 \pm 0.0002$

Table 4: Values of Boltzmann's constant and drag coefficient, as found from the fit parameters of PSD. See Section 4.2 for the equations used to find them.

Axis	Intensity	PSD method [pN/ $\mu$ m]	Energy method [pN/ $\mu$ m]	Equipartition method [pN/ $\mu$ m]
X	100 mA	29.0 $\pm$ 0.9	8.7 $\pm$ 0.2	8.1 $\pm$ 0.2
	150 mA	42 $\pm$ 1	10.5 $\pm$ 0.3	10.6 $\pm$ 0.3
	200 mA	57 $\pm$ 2	15.3 $\pm$ 0.6	13.7 $\pm$ 0.4
	250 mA	63 $\pm$ 4	13.4 $\pm$ 0.3	13.4 $\pm$ 0.3
	300 mA	61 $\pm$ 3	17.1 $\pm$ 0.5	16.1 $\pm$ 0.5
Y	100 mA	13.8 $\pm$ 0.4	102 $\pm$ 6	106 $\pm$ 6
	150 mA	17 $\pm$ 5	133 $\pm$ 8	126 $\pm$ 7
	200 mA	63 $\pm$ 7	300 $\pm$ 20	320 $\pm$ 20
	250 mA	64 $\pm$ 6	350 $\pm$ 20	350 $\pm$ 20
	300 mA	61 $\pm$ 5	430 $\pm$ 20	420 $\pm$ 20

Table 5: Trap stiffness along X and Y, as found by the three methods described in Section 3.2.2.

## 5. Discussion

### 5.1. Discussion of calibration results

In this section we describe features of our calibration procedure and how these can give rise to uncertainty in our measurements. Namely we will explain qualitative features of the raw and processed signals, as well as understand the sources of error in our fit parameters.

#### 5.1.1. Error Analysis on Stage Calibration

To obtain the error values seen in Fig. 10 for the voltage as a function of position we used standard statistical analysis techniques to calculate the standard error of the fit parameters  $\alpha$ . Specifically we used (29) for the gradient error and (30) for the intercept error.

$$\alpha_{fit} = \sqrt{\frac{1}{N-1} \sum_i (y_i - m x_i - c)^2} \quad (28)$$

$$\alpha_m = \alpha_{fit} \sqrt{\frac{N}{\Delta}} \quad (29)$$

$$\alpha_c = \alpha_{fit} \sqrt{\frac{\sum_i x_i^2}{\Delta}} \quad (30)$$

$$\Delta = N \sum_i x_i^2 - \left( \sum_i x_i \right)^2 \quad (31)$$

where  $N$  is the number of data points,  $x_i$  and  $y_i$  are the x and y values of the  $i$ th data point respectively, while  $m$  and  $c$  are the linear fit parameters. Equations (29) and (30) are simply the least square regression errors on the fit parameters. Since this does not take into account the intrinsic uncertainty of our experimental data (e.g. the error in the reading scale of the micrometer, the fluctuation in the applied voltage, etc.) we have calculated  $\chi^2$  with (32) for both fits in order to evaluate a confidence level in our model.

$$\chi^2 = \sum_i \left( \frac{y_i - m x_i - c}{\alpha_i} \right)^2 \quad (32)$$

where  $\alpha_i$  is the standard error of the  $i$ -th data point.

As a result the fit in Fig. 10 (a) has a p-value of 0.95 while the one at (b) has a p-value of 0.80. Considering the limited number of data point we feel confident in calibrating our QPD with these values across position. Given more time, a more thorough data collection with a smaller step is encouraged to decrease uncertainty.

#### 5.1.2. Qualitative Description of QPD Waveform

A sample signal of the motion of the stage, including the QPD's response is shown on the left side of Fig. 11. The upper subfigure depicts (in black) the motion of the stage in the x-axis over time, while the x-axis QPD response (in blue) is depicted below that. One might expect that there should be a 1-1 correlation of these two signals when depicted on the same time axis. However, this does not seem to be the case for any of our signals (look at Fig. B.14a and Fig. B.14b for the rest of the trials). This is expected, as the size of the bead is smaller than the displacement of the stage. As a result the bead is moving in and out of the trap throughout the stage motion as seen in Fig. 13.

To specifically explain how we get the periodic signal with 4 peaks seen in Fig. 11 we will explain the process shown in Fig. 13. We start at subfigure (a) where the bead is at the left of the trap. Hence, all of the light from the trap is reaching the QPD undeflected producing a flat singal (seen on the left). When the bead moves partially into the trap (b) it's circular geometry refracts a portion of the light away from trap's focal point. This causes less light from the left side of the trap to reach the QPD. As a result it seems as if the QPD is detecting motion to the left, resulting in the long dip in the signal. When the trap is completely inside the bead (c) the QPD works normally, i.e. a deflection to the right (from equilibrium) corresponds to a sharp increase in signal, while a deflection to the left corresponds to a sharp decrease. Finally the bead moves away from equilibrium (d) and the process occurs in reverse producing a reflected (about the equilibrium) signal.

This is the reason why we developed an algorithm to detect the flat regions where the bead was within the QPD in order to properly calibrate. This algorithm and an implementation is fully described in Appendix C.

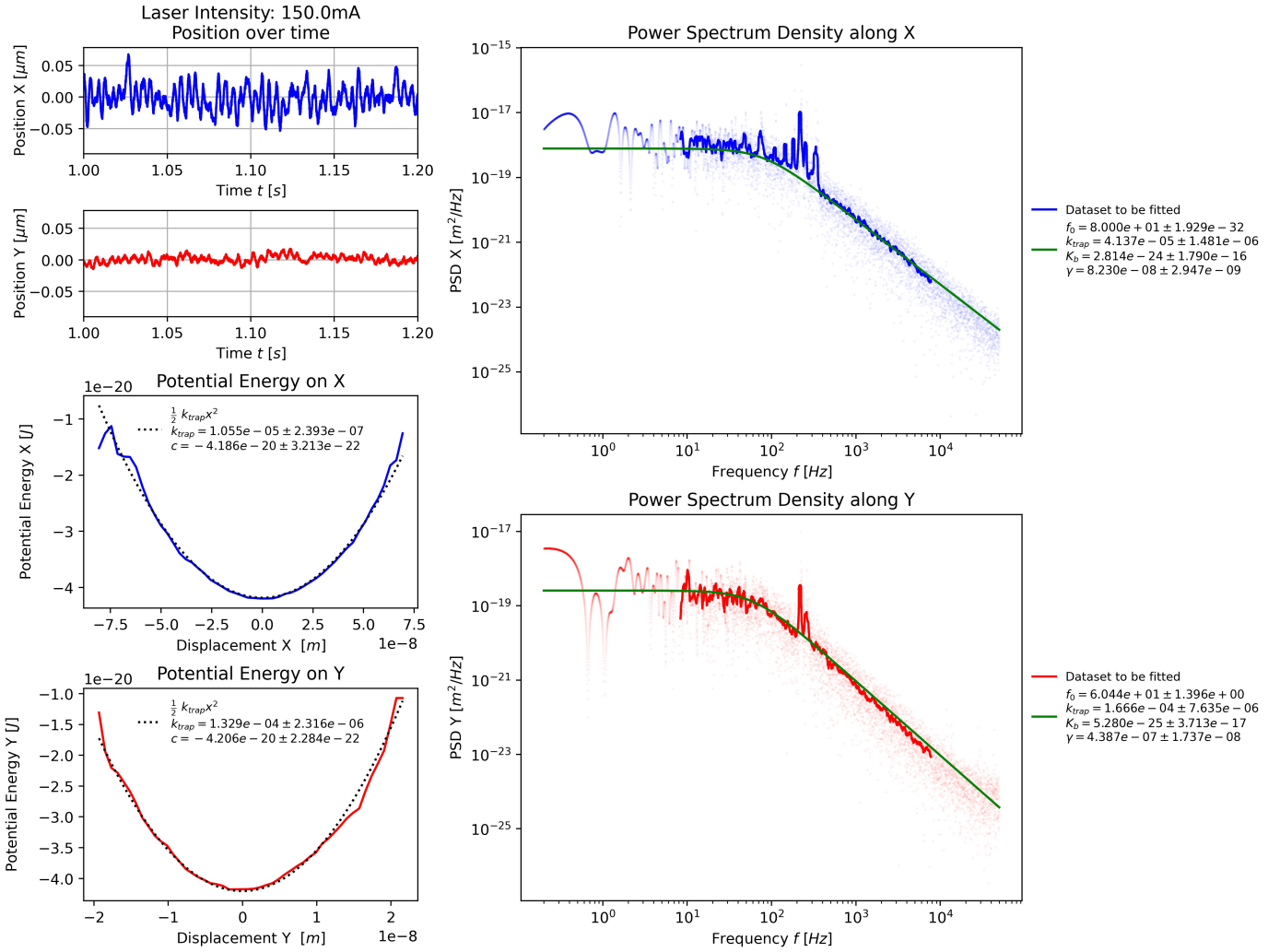


Figure 12: Time-series of position, power spectrum density and potential energy for X and Y axis at 150.00mA. Blue graphs refer to X axis, red graphs to Y axis. The PSD graph on the right shows the rescaled data in pale blue/red and the portion of the moving average dataset that was fit in solid blue/red. The reader is encouraged to look at Appendix D for the complete plot.

### 5.1.3. Suggestions for improving QPD Calibration

Here we discuss possible sources of the systematic and random errors that are present in the calibration data, as well as provide suggestions on what experimental procedures could be used to circumvent them.

As illustrated across the report, and especially in section 3.1.3, due to significant spherical aberration of the trap laser, we were unable to achieve high trapping efficiency in the z-axis. This lead to not being able to concretely identify at what focal plane does a bead coincide with the trap's center. Thus systematic error was introduced in our calculations for the x-y QPD-Stage calibration as we did not know the z-distance between the trap's center and the stuck bead.

To circumvent this issue we suggest that the calibration procedure described in section 3.2.1 is repeated for a step on the z-axis. Collecting such data will allow one to qualitatively compare the QPD signals for the z-axis at multiple values, and select the one where the bead coincides with the trap. Such a signal is supposed to contain only peaks interrupted with flat periods.

Once one identifies such a height they will be able to conduct a more accurate calibration of the instrument.

## 5.2. Discussion of Trapped Bead Calibration

### 5.2.1. Error Calculations

The fitting for PSD and potential energy was done with non-linear least square fitting. The error bars on the fit parameters ( $A, f_0$  from PSD and  $k_{trap}$  from energy) were all taken directly from the estimated covariance matrix that the Python `curve_fit` function generates:  $\begin{pmatrix} \sigma_a^2 & \sigma_{ab} \\ \sigma_{ba} & \sigma_b^2 \end{pmatrix}$ . That is, the error bar for a fit parameter is the square root of the relevant element in the main diagonal of the covariance matrix.

For the Boltzmann's constant and drag coefficient, the errors were propagated from the errors on the fit parameter  $A$ , as follows:

$$\sigma_\gamma = \gamma \frac{\sigma_A}{A} \quad (33)$$

$$\sigma_{k_B} = \frac{3\pi^3 \eta d}{T} \sigma_A \quad (34)$$

The errors on the trap stiffness found from PSD was propagated from the errors on the fit parameters A and  $f_0$ :

$$\sigma_{k_I} = \sqrt{\left(2\pi\gamma\sigma_{f_0}\right)^2 + \left(k_{trap} \frac{\sigma_\gamma}{\gamma}\right)^2} \quad (35)$$

The errors on the trap stiffness from the potential energy and equipartition theorem were propagated from the error in QPD calibration, as follows:

$$\sigma_{k_{II,III}} = 2k_{trap} \sqrt{\left(\frac{\sigma_\alpha}{\alpha}\right)^2 + \left(\frac{\sigma_\beta}{\beta}\right)^2} \quad (36)$$

For the trap stiffness found from the fit of potential energy, the propagated error was compared with the error from the covariance matrix and the bigger one was taken.

### 5.2.2. Discussion of PSD fitting

At first we attempted to fit the PSD with only one free parameter (trap stiffness) by rewriting the corner frequency in terms of the trap stiffness and assuming a theoretical drag coefficient, but the range of functions defined this way didn't fit the data indicating that one parameter is not sufficient to describe such a function mathematically. This is why we used two parameters instead although the physical values of the two are related. We tried several methods of function fitting in Python but the non-linear least-square fitting method with `curve_fit` gave the best results. In order to arrive to a good fit we varied the suggested initial boundaries for each parameter. We did this by starting with a large range and then narrowing it down to get a fit that appears visually best (most of the fits would be very visibly not a good fit to the data). This procedure may have introduced some bias in selecting ranges of values for the parameters. To eliminate this, we recommend using the values of trap stiffness and drag coefficient found with other methods to choose the ranges of values or searching for more automated procedures that improve the `curve_fit` method.

### 5.2.3. Discussion of Boltzmann's constant and drag coefficient

The values found for Boltzmann's constant and drag coefficient were not in agreement with the theoretical value (a t-score  $> 3$ , assuming a theoretical value with no error). From the data analysis, this could potentially be due to underestimated error bars, unaccounted error bars on temperature or bad fitting. Additionally, the temperature here was assumed to be room temperature but in reality the value is different because the laser heats the environment around the bead. We tried to plot the expected PSD curves with the trap stiffness found by the other two methods and theoretical drag coefficient, and we found that the PSD values are a couple order of magnitudes larger (see [Appendix D](#)) than the obtained data. This might be because of a

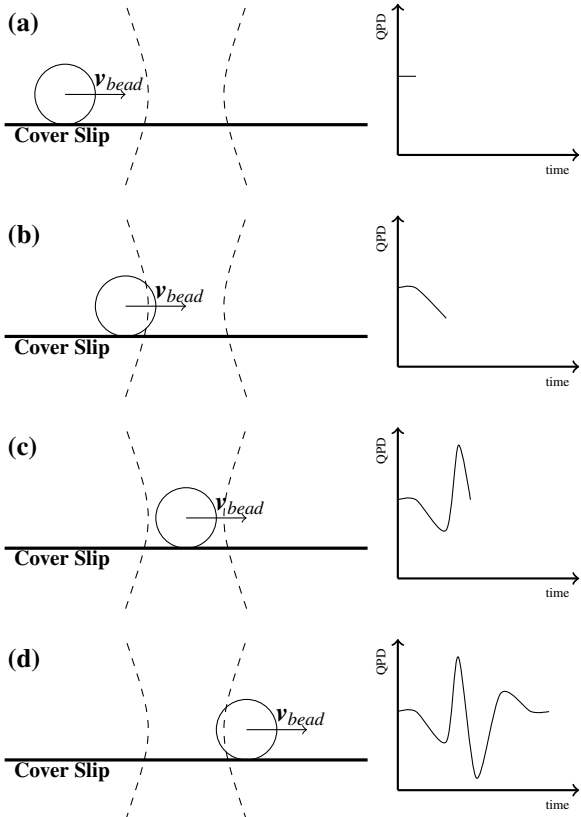


Figure 13: Visual explanation of the signal received as the node passes through the trap (denoted in dashed lines). The progression starts at (a) with the bead moved outside the trap and finishes at (d) with the bead having traversed through the beam. On the right of each frame is a plot of the QPD signal received along this axis. The progression is analytically explained in section 5.1.

mistake in the code generating the PSD or because indeed the drag coefficient is different than the expected one for water. We found no mistakes in the code so a next step would be to either try constructing the PSD with other methods or check again the code and understanding of the current method. A measurement of the drag coefficient by driving the stage of a trapped bead can also be performed to evaluate this explanation.

#### 5.2.4. Discussion of Trap Stiffness in X and Y

From the time series graphs (see Appendix D, one can see a difference in the amplitude of oscillation between the X and Y axes. This was confirmed by performing a t-test comparing the trap stiffness in X and Y, for each laser power and for the equipartition and potential energy method separately. A different stiffness coefficient for each axis is unexpected and may be due to: (1) a mistake in the procedure or setup - this can be easily checked by redoing the experiment which we did not have time to do as our time on the experiment had ended when we saw this difference; (2) if the intensity of the laser changes differently in X vs Y or if the shape of the beam is an ellipse - this is also unlikely as such features were not identified at the final time of setting up and aligning the laser; (3) if the equilibrium position for the bead is not at the center of the focus in the XY-plane, but we see no reason for this to be happening; (4) if the laser is not entirely vertical but at an angle. If redoing the experiment doesn't solve this difference we recommend investigating further option (4) and theoretically investigating possible explanations.

## 6. Conclusion

We have assembled an optical tweezers kit from Thorlabs. The QPD was calibrated in axes X and Y to convert the voltage into position data. The trap stiffness was found along X and Y with three methods: fitting the power spectrum density, fitting the potential energy histogram constructed from the time series and using the equipartition theorem. The Boltzmann's constant and drag coefficient found from PSD fitting were inconsistent with theoretical values, pointing at either a mistake in the code or an actually different value of the drag coefficient. The trap stiffness found with the other two methods was different along X and Y which was unexpected so we recommend redoing the measurement or further investigating the reasons behind this difference before performing force measurement with it. At this moment, the focal point of the laser and objective are not coinciding and a bead cannot be trapped in the Z axis. Further investigation of this issue can improve the instrument operation and allow to measure forces in this axis too.

## References

- [1] J. Molloy, and M. Padgett. Lights, action: Optical tweezers. *Contemporary physics*, 43(4):241–258, 2002.
- [2] P. Polimeno, A. Magazza, M.A. Iati, F. Patti, R. Saija, C.D.E. Boschi, M.G. Donato, P.G. Guciardi, P.H. Jones, G. Volpe, et al. Optical tweezers and their applications. *Journal of Quantitative Spectroscopy and Radiative Transfer*, 218:131–150, 2018.
- [3] T. T. Perkins. Optical traps for single molecule biophysics: A primer. *Laser & Photonics Reviews*, 3(1-2):203–220, 2009.
- [4] J.R. Moffitt, Y. R. Chemla, S. B. Steven, and C. Bustamante. Recent advances in optical tweezers. *Annu. Rev. Biochem.*, 77:205–228, 2008.
- [5] T.A. Nieminen, N. du Preez-Wilkinson, A. B. Stilgoe, V. LY. Loke, A. AM. Bui, and H. Rubinsztein-Dunlop. Optical tweezers: Theory and modelling. *Journal of Quantitative Spectroscopy and Radiative Transfer*, 146:59–80, 2014.
- [6] Keir C. Neuman and Steven M. Block. Optical trapping. *The Review of scientific instruments*, 75(9):2787–2809, Sep 2004. 16878180[pmid].
- [7] E.M. Purcell and D.J. Morin. *Electricity and Magnetism*. Electricity and Magnetism. Cambridge University Press, 2013.
- [8] Yasuhiro Harada and Toshimitsu Asakura. Radiation forces on a dielectric sphere in the rayleigh scattering regime. *Optics Communications*, 124(5):529–541, 1996.
- [9] D.J. Griffiths. *Introduction to Electrodynamics*. Number v. 2. Cambridge University Press, 2017.
- [10] Thorlabs. Modular optical tweezers. [https://www.thorlabs.com/NewGroupPage9.cfm?ObjectGroup\\_ID=3959](https://www.thorlabs.com/NewGroupPage9.cfm?ObjectGroup_ID=3959). (Accessed on: 03/07/2021).
- [11] Thorlabs. Modular tweezers otkb(m): User guide. <https://www.thorlabs.com/drawings/f5756282cf645a45-20CB384D-0862-22BD-8ABF17EFB3074C5F/OTKB-Manual.pdf>. (Accessed on: 03/09/2021).
- [12] Thorlabs. Back focal plane detection module for otkb(m): User guide. <https://www.thorlabs.com/drawings/e246b1b3d612b7e7-90714998-D856-B4A2-EFA2AF20C4CEC029/OTKBFM-Manual.pdf>. (Accessed on: 03/13/2021).
- [13] P. Oikonomou and M. Filova. Advanced lab. <https://github.com/PanosEconomou/advanced-lab>, 2021.
- [14] Thorlabs. Imaging/focusing microscope objectives, oil immersion. [https://www.thorlabs.com/newgroupage9.cfm?objectgroup\\_id=1018&pn=N100X-PFO](https://www.thorlabs.com/newgroupage9.cfm?objectgroup_id=1018&pn=N100X-PFO). (Accessed on 03/05/2021).
- [15] David C Appleyard, KY Vandermeulen, H Lee, and Matthew J Lang. Optical trapping for undergraduates. *American journal of physics*, 75(1):5–14, 2007.
- [16] Thorlabs. Fluorescing alignment disks for ir source. [https://www.thorlabs.com/newgroupage9.cfm?objectgroup\\_id=3201&pn=VRC4CPT#11307](https://www.thorlabs.com/newgroupage9.cfm?objectgroup_id=3201&pn=VRC4CPT#11307). (Accessed on: 03/24/2021).
- [17] M. Born and E. Wolf. *Principles of Optics: Electromagnetic Theory of Propagation, Interference and Diffraction of Light*. Elsevier Science, 2013.
- [18] ibidi. Microscopy parameters of cell culture surfaces — ibidi. <https://ibidi.com/content/209-microscopy-parameters-of-materials>. (Accessed on 03/05/2021).
- [19] Erik Schäffer. Handout for optical tweezers practical course: Optical tweezers calibration. <https://idisk-srv1.mpi-cbg.de/~diez/Practical%20handout%20schaeffer.pdf>. (Accessed on: 04/01/2021).
- [20] Physics 111B: Advanced Experimentation Laboratory. OTZ - Optical Trapping. University of California, Berkeley. <http://experimentationlab.berkeley.edu/sites/default/files/writeups/OTZ.pdf> (Accessed on: 03/28/2021).
- [21] Junior Lab. Optical Trapping. MIT Department of Physics. <https://ocw.mit.edu/courses/physics/8-13-14-experimental-physics-i-ii-junior-lab-fall-2016-spring-2-experiments/optical-trapping/> (Accessed on: 03/28/2021).
- [22] F. Reif. *Fundamentals of Statistical and Thermal Physics*. McGraw-Hill, 1965.
- [23] OM Solomon Jr. Psd computations using welch's method. *NASA STI/Recon Technical Report N*, 92, 1991.

## Appendix A. Detailed Procedure for Calibration

### Appendix A.1. Stage and QPD Calibration

Section 3.2.1 briefly summarized the method to obtain the two conversion factors:  $\alpha$  - the QPD-stage voltage conversion factor and  $\beta$  - the stage position-voltage conversion factor. More specifically, these are the steps we followed:

1. Prepare a solution of silica beads (diameter  $2\mu m$ ) in PBS with 1:10k dilution. PBS, which stands for phosphate-buffered solution, is used to fixate the beads to one of the two surfaces of the sample (slide or coverslip). The ions of the PBS solution stick to the bead surface, making it positively charged and therefore attracted to the negatively charged glass surface. The PBS buffer and beads solution were provided by Prof. Shubeita.
2. Prepare a slide with a flow channel containing the prepared solution. The procedure we used to do this can be found in [21].
3. Place the slide on the stage. Focus the microscope and position the stage such that a stuck bead is at the location of the laser as seen on the camera.
4. Select the position in Z to be approximately the same as the one used to perform the optical trap calibration, i.e. such that the image of the bead is as focused as it was in the trap calibration.
5. Using LabVIEW, move the stage with a triangular wave of frequency 10 Hz and amplitude  $2 \mu m$  for 5 seconds.
6. To ensure that the bead is at the center of the trap: check if the QPD is properly aligned, and adjust the position of the stage until driving the stage in the X direction produces no change in the Y direction.
7. Record and save the QPD and strain gauge data of such movement.
8. Repeat the data collection for several laser powers, which are used for the optical trap calibration (100mA, 150mA, 200mA, 250mA, 300mA).
9. Center the stuck bead at the laser trap again. Using LabVIEW send a voltage pulse that moves the stage for a certain distance.
10. Find the distance the stage moved: read the stage position at the new position, move the differential micrometers until the bead is at the center again and read the new position.
11. Repeat this for pulses with different amplitudes (3V, 5V, 7V, 9V, 10V).
12. Repeat all steps separately for movement in X and movement in Y. Changing the axis along which the stage is driven requires to move the input cable from the piezo controller K-cube for X to the piezo controller K-cube for Y.

### Appendix A.2. Optical Trap Calibration

Here we provide the step-by-step procedure used to collect time series data of a trapped bead, as described in Section 3.2.2.

1. Prepare a solution of silica beads (diameter  $2\mu m$ ) in water with 1:50k dilution. Such low dilution is necessary so that the trap attracts only one bead for a prolonged time.
2. Prepare a slide with a flow channel containing the prepared solution. The procedure we used to do this can be found in [21].
3. Place the slide on the stage. Focus the microscope on the sample and trap a bead. The bead may be repelled at first so it may be necessary to "catch" it by moving the stage.
4. Bring the bead at approximately the Z position that was found to be closest to the centre of the trap in Section 3.1.3.
5. Using LabVIEW record time series data for several laser powers (100mA, 150mA, 200mA, 250mA, 300mA). LabVIEW immediately displays the data so for each laser power we made sure the data provides a good potential curve.

## Appendix B. QPD Calibration Data

Here we cite the full plots for the QPD Calibration for both X and Y axes. The method to obtain such plots is described in Section 4.1. We remind the reader that all the data can be found [here](#) along with the code on how to generate such plots.

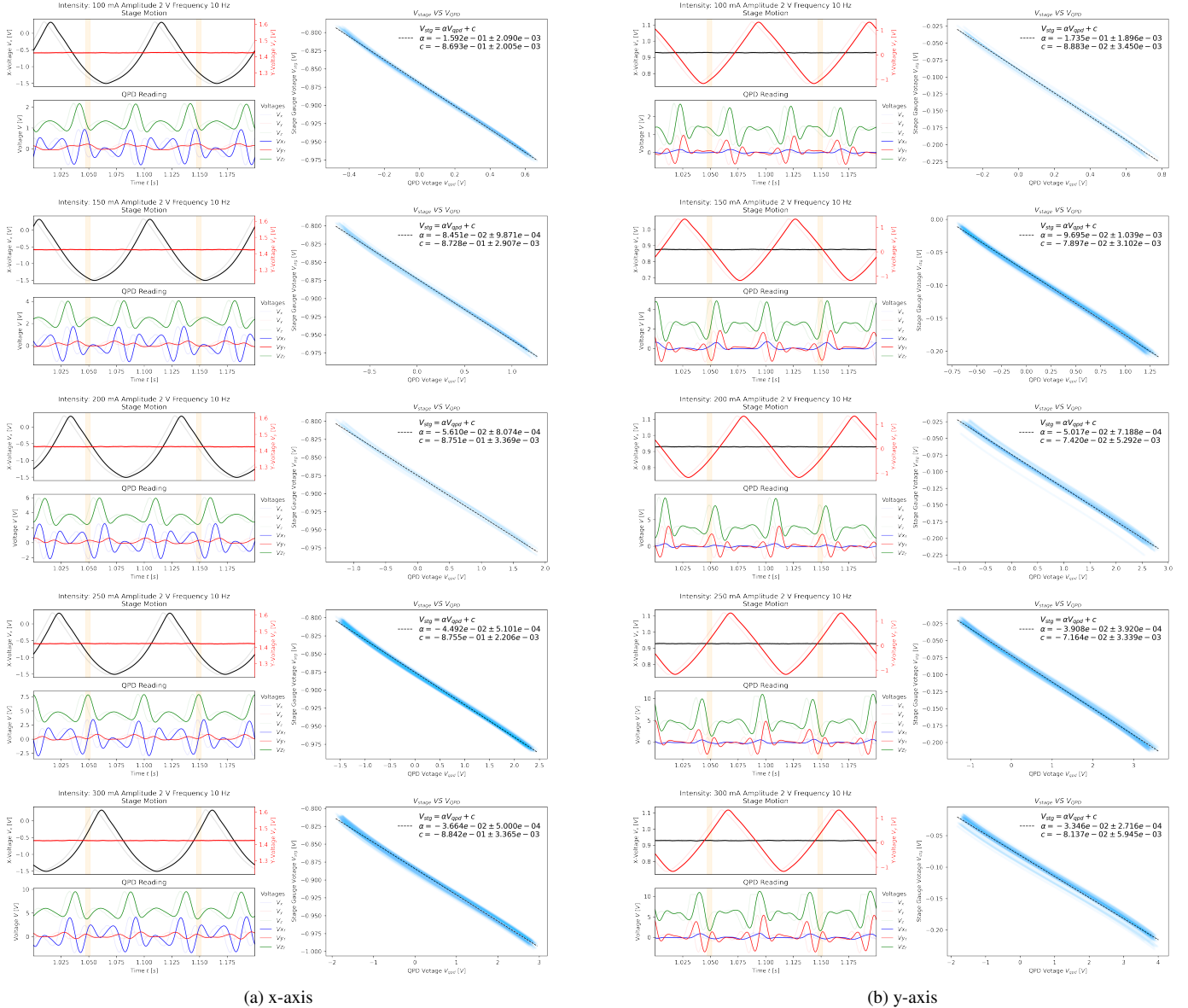


Figure B.14: The full calibration of the x and y of the QPD output for multiple laser intensities.

## Appendix C. Algorithm for Detecting Flat Regions

Here we describe the algorithm we designed and implemented to detect the flat regions in the QPD Signal. The full implementation can be found [here](#). An abstract reasoning of how the selection algorithm works is given in section 4.1. The code described in this section is given below in an encapsulated form.

```

1 # Function to receive a data set and return a set of all the regions where the positions are inside
2 # the trap.
3 def split(data_qpd,data_stg,time,fc=100,order=1,grad_min = 0.75, grad_max = 1, time_max=0.001,
4 time_min = 0,tolerance=0.05,trigger='rising'):
5     # Filter out the high frequencies
6     # Filter parameters
7     fs = len(time)/(max(time)-min(time))      # Sampling Frequency
8     fc = 100                                     # Cutoff frequency
9     order = 1                                    # Order
10
11    # Pass everything through the filter
12    data_qpd1 = butter_lowpass_filter(data_qpd,fc,fs)
13    data_stg1 = butter_lowpass_filter(data_stg,fc,fs)
14
15    # Take the derivative
16    data_qpd2 = derivative(data_qpd1,fs=fs)
17    data_qpd2/=max(data_qpd2[1:len(data_qpd2)-1])      # Normalize the derivative
18
19    # Identify the regions of straight lines
20    pairs = intersection_points(data_qpd2,limit=grad_min,trigger=trigger) # Get the pairs
21    pairs = filter_amplitude(data_qpd2,pairs,limit=grad_min,DA=abs(grad_max-grad_min),tolerance=
22 tolerance)      # Filter them by amplitude
23
24    # Now obtain the two segmented lists
25    return [superpose(data_qpd1,pairs), superpose(data_stg1,pairs), pairs]

```

Listing 1: Block Level of final detection function

We have written every function seen above. In the following we provide the function intersection points which takes in the filtered derivative of the data ad returns a set of tuples of time coordinates during which the x-value is in between a set point in the derivative. The two functions below that are functions that filter that set of tuples to ensure data integrity by removing small time gaps or large amplitude gaps.

```

1 # This will return a set of pair witch will be all segments above the limit or below the limit
2 # depending on the trigger mode.
3 def intersection_points(in_data,limit,trigger='rising'):
4     data = in_data - limit
5     indx = []
6     rising = (trigger == 'rising') # is the next one I am expecting rising?
7     pair = []
8     intcnt = 0
9     for i in range(len(data)-1):
10         if data[i]*data[i+1] <= 0:
11             intcnt += 1
12
13             if rising == (data[i] < data[i+1]):
14                 rising = not rising
15                 if len(pair) == 0:
16                     pair.append(i)
17                 else:
18                     pair.append(i)
19                     indx.append(pair)
20                     pair = []
21     return np.array(indx)
22
23 # This function will receive the set of pairs and it will select the ones who's time separation is
24 # within a predefined range Dt.
25 def filter_time(time,pairs,Dt=1,tolerance=0.1):
26     return np.array([pair for pair in pairs if abs(time[pair[1]]-time[pair[0]]) - Dt) < tolerance])
27
28 # Receives a set of pairs and will select the ones who do not cross a specific amplitude
29 def filter_amplitude(data,pairs,limit,DA=1, tolerance = 0.1):
30     return np.array([pair for pair in pairs if abs(max(abs(data[pair[0]:pair[1]])-limit)) - DA) <
31 tolerance])

```

Listing 2: Pairs detection functions

## Appendix D. Trapped Bead Calibration Data

Here we cite the full plots for the Trapped Bead Calibration in X and Y axes. The method to obtain such plots is described in Section 4.2. We remind the reader that all the data and figures can be found [here](#).

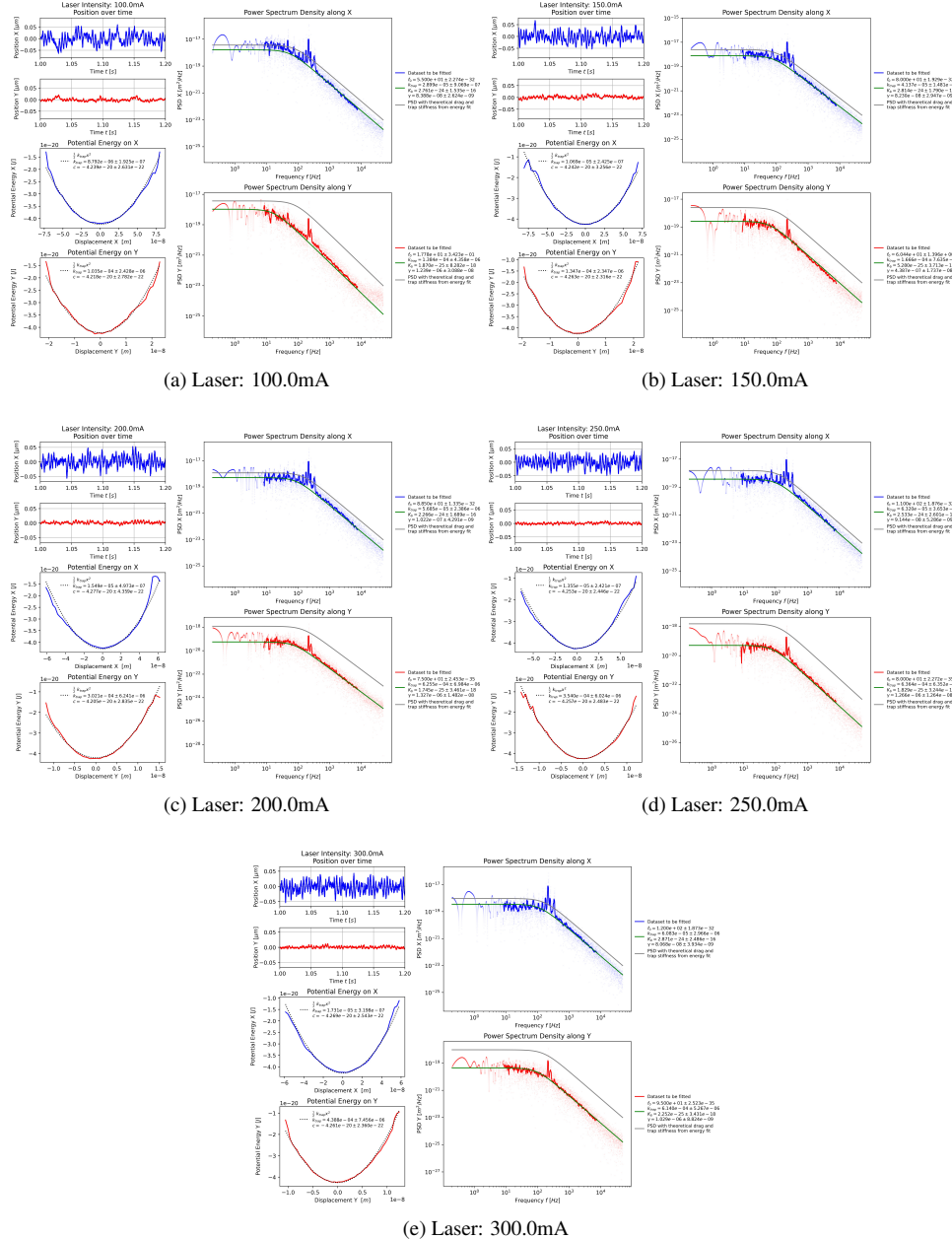


Figure D.15: The set of plots for calibrating the trap stiffness for a trapped bead